TABLE 1 P Cygni's mean light curve from 1700 to 1990

Date (yr)	Epoch (yr)	Mag (V)	Number of observations
1704–1715	1712	5.23 ± 0.15	4
1746–1754	1750	5.15 ± 0.07	2
1779–1795	1791	5.12 ± 0.27	8
1814–1843	1833	5.07 ± 0.06	3
1872–1882	1878	4.97 ± 0.06	3
1884–1897	1891	4.95 ± 0.09	7
1898–1917	1906	4.92 ± 0.08	3
1952–1954	1953	4.83 ± 0.01	?
1965–1966	1966	4.80	2
1982	1982	4.83 ± 0.05	11
1985–1990	1988	4.82 ± 0.01	476

expanding so that the star moves to the right in the HRD at constant luminosity. The second crossing occurs in a later phase when the star has lost so much mass that it can no longer sustain an extended convective envelope above the H-burning shell. In that phase the envelope contracts and the star moves to the left of the HRD to become a Wolf–Rayet star.

The observed decrease of $T_{\rm eff}$ shows that P Cyg is in the expansion phase after the main sequence. This expansion is expected to occur on the Kelvin–Helmholtz timescale for contraction

$$\tau_{\rm KH} = GM^2/R_* L \approx 520\ {\rm yr} \qquad (3)$$

which is of the same order of magnitude as the observed timescale of the increase of R_*, of $\tau(R_*) = 320$ yr. This supports the suggestion that the star is in the H-shell burning phase.

The predicted evolutionary speed of a star with the luminosity of P Cygni in the H-shell burning phase near $T_{\rm eff} = 20{,}000$ K is $d \log(T_{\rm eff})/dt = -0.013$ per century[3], which implies a decrease in $T_{\rm eff}$ of only 3% per century. This is about half the observed value of 6% per century. So the observed evolution speed of P Cyg is twice as fast as predicted. The discrepancy between the ob-served and predicted evolutionary speed might be due to two effects: (1) The calculated evolutionary speed might be wrong because the outer layers of the star expand faster than predicted. In fact, recent calculations of the evolution of luminous stars by A. Maeder (personal communication) suggest that dynamical effects due to radiation pressure in the envelope of the star result in a more rapid expansion of the star and consequently also in a more rapid decrease in $T_{\rm eff}$ than predicted by the quasi-hydrostatic evolution calculations[3]. (2) The mass of the star, derived from its luminosity, might be overestimated. In fact, Pauldrach and Puls[14] derived a surface gravity for P Cyg of $\log g = 2.04 \pm 0.01$ from detailed modelling of its stellar wind. Assuming a luminosity of $\log L/L_\odot = 5.86 \pm 0.1$, they derived a mass of $M = 23 \pm 2\ M_\odot$. This is about a factor of 0.6 smaller than the mass of $40 \pm 4\ M_\odot$ derived from the predicted evolution for a star of P Cyg's $T_{\rm eff}$ and L if it is evolving to the right in the HRD[15]. If the core mass is also smaller than predicted, by the same factor of 0.6, the timescale for the core contraction and the envelope expansion will be about a factor two shorter than predicted by the evolutionary calculations of Maeder and Meynet[3], as this timescale is proportional to $M^2_{\rm core}$. This would bring the predicted timescale for the expansion into agreement with the observed brightening of P Cyg. □

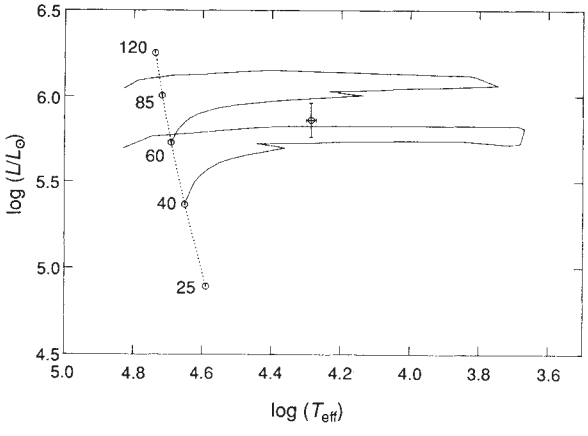

FIG. 2 Location of P Cyg in the Hertzsprung–Russell diagram compared with the predicted evolutionary tracks[15] of two stars with initial masses of 40 and 60 $M_\odot$. The zero-age main sequence (dotted) for stars of various initial masses is also shown. The observed visual brightening of P Cyg indicates that it is evolving to the right in this diagram at a rate twice as large as predicted by models of stellar evolution.

Received 21 October; accepted 15 November 1991.

1. de Jager, C. *The Brightest Stars*, 100 (Reidel, Dordrecht, 1980).
2. Lamers, H. J. G. L. M., de Groot, M. J. H. & Cassatella, A. *Astr. Astrophys.* **128,** 299–310 (1983).
3. Maeder, A. & Meynet, G. *Astr. Astrophys.* **182,** 243–263 (1987).
4. Mueller, G. & Hartwig, E. in *Geschichte und Literatur des Lichtwechsels der Veränderlichen Sternen*, 444 (Universitätssternwarte Berlin-Babelsberg, 1918).
5. Prager, R. in *Geschichte und Literatur des Lichtwechsels der Veränderlichen Sternen*, 61 (Universitätssternwarte Berlin-Babelsberg, 1936).
6. Schneller, R. in *Geschichte und Literatur des Lichtwechsels der Veränderlichen Sternen*, 258 (Akademie, Berlin, 1957).
7. De Groot, M. J. H. in *Physics of Luminous Blue Variables* (eds Davidson, K. *et al.*) 257–258 (Kluwer, Dordrecht, 1989).
8. Hiltner, W. A. *Astrophys. J. suppl. Ser.* **2,** 389–399 (1956).
9. Johnson, H. L. & Mitchell, R. I. *Rev. Mex. Astr. Astrofis.* **1,** 299–324 (1975).
10. Mitchell, R. I. & Johnson, H. L. *Comm. lunar planet. Lab.* **8,** 1–49 (1970).
11. Percy, J. R. & Welch, D. L. *Publ. astr. Soc. Pacific* **95,** 491–505 (1983).
12. Percy, J. R. *et al. Astr. Astrophys.* **191,** 248–252 (1988).
13. Schmidt-Kaler, Th. in *Landolt-Bornstein, New Series, Group VI*, Vol. 2b, 452 (Springer, Berlin, 1982).
14. Pauldrach, A. W. A. & Puls, J. *Astr. Astrophys.* **237,** 409–424 (1990).
15. Maeder, A. *Astr. Astrophys. Suppl.* **84,** 139–177 (1990).

Territory covered by *N* diffusing particles

Hernan Larralde*, Paul Trunfio*, Shlomo Havlin*†, H. Eugene Stanley* & George H. Weiss†

* Center for Polymer Studies and Department of Physics, Boston University, Boston, Massachusetts 02215, USA
† Physical Sciences Laboratory, Division of Computer Research and Technology, National Institutes of Health, Bethesda, Maryland 20892, USA

THE number of distinct sites visited by a random walker after t steps is of great interest[1–21], as it provides a direct measure of the territory covered by a diffusing particle. Thus, this quantity appears in the description of many phenomena of interest in ecology[13–16], metallurgy[5–7], chemistry[17,18] and physics[19–22]. Previous analyses have been limited to the number of distinct sites visited by a single random walker[19–22], but the (nontrivial) generalization to the number of distinct sites visited by N walkers is particularly relevant to a range of problems—for example, the classic problem in mathematical ecology of defining the territory covered by N members of a given species[13–16]. Here we present an analytical solution to the problem of calculating $S_N(t)$, the mean number of distinct sites visited by N random walkers on a d-dimensional lattice, for $d = 1$, 2, 3 in the limit of large N. We confirm the analytical arguments by Monte Carlo and exact enumeration methods. We find that there are three distinct time regimes, and we determine $S_N(t)$ in each regime. Moreover, we also find a remarkable transition, for dimensions ≥ 2, in the geometry of the set of visited sites. This set initially grows as a disk with a relatively smooth surface until it reaches a certain size, after which the surface becomes increasingly rough.

The formalism used to obtain the analytical results, and on which the exact enumeration[20] calculations are based, is as follows. We denote the probability that a single random walker

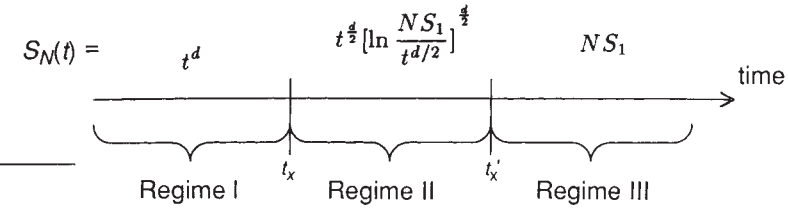

FIG. 1 Schematic illustration of the results for the number of distinct sites visited by N random walkers initially at the origin, indicating the fact that at different times t the behaviour is very different. Here, S_1 is given by equation (7).

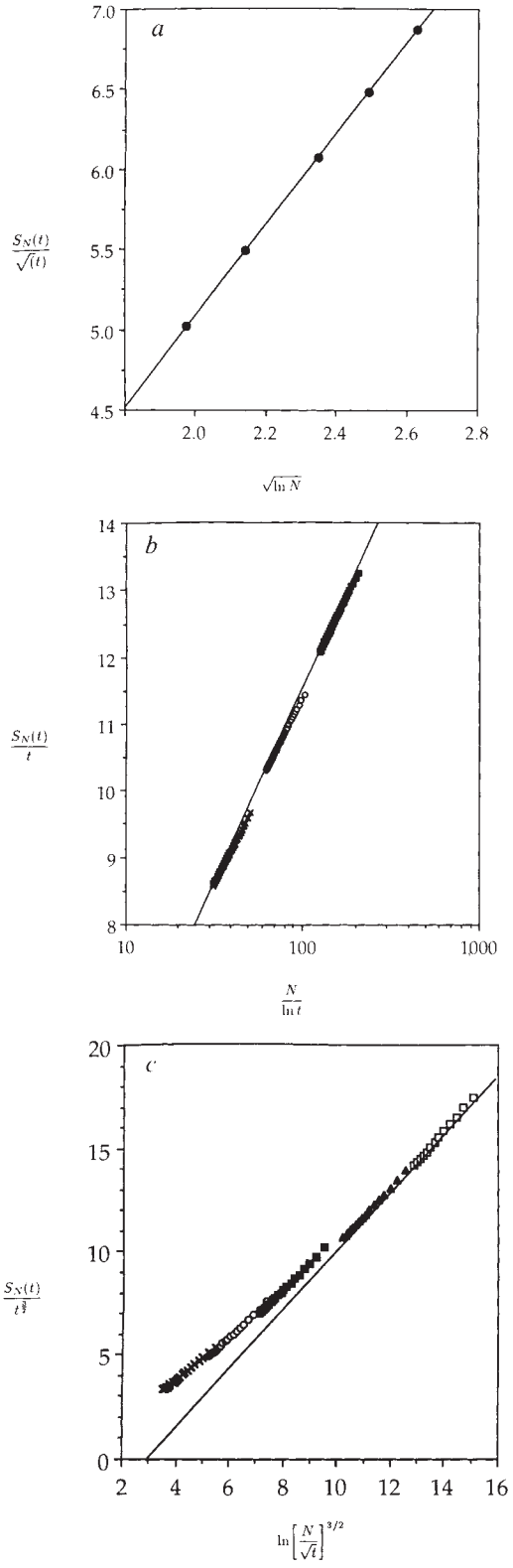

FIG. 2 Scaling plot demonstrating that equation (4) holds for (*a*) a one-dimensional system ($d=1$), (*b*) a two-dimensional system ($d=2$) and (*c*) a three-dimensional system ($d=3$). Each data point in *a* and each of the different symbols in *b* and *c* correspond to different values of N.

is at site $\mathbf{r}$ for the first time at step t by $f_t(\mathbf{r})$, and the probability that site $\mathbf{r}$ has not been visited by this walker by step t as $\Gamma_t(\mathbf{r})$. Then

$$\Gamma_t(\mathbf{r}) = 1 - \sum_{t'=0}^{t} f_{t'}(\mathbf{r}) \tag{1}$$

Because the N walkers are independent, the probability that site $\mathbf{r}$ has not been visited by any of the N random walkers is $[\Gamma_t(\mathbf{r})]^N$. The probability that site $\mathbf{r}$ has been visited by at least one walker by step t is $1-[\Gamma_t(\mathbf{r})]^N$. Thus the expected number of distinct sites visited by any of the N random walkers by step t is obtained by summing over all sites $\mathbf{r}$ in the lattice

$$S_N(t) = \sum_{\mathbf{r}} \{1 - [\Gamma_t(\mathbf{r})]^N\} \tag{2}$$

We can now analyse the very short time behaviour of $S_N(t)$ (regime I; see Fig. 1). As N tends to infinity, any number raised to the power N approaches zero if the number is less than one; hence $[\Gamma_t(\mathbf{r})]^N$ tends to zero if it is possible that a walker may arrive at site $\mathbf{r}$ by step t. From equation (2) we see that $S_N(t)$ consists of all the sites that have non-zero probability of being visited by step t, and is therefore independent of N. As the walker can take only nearest-neighbour steps, it follows that for large N, $S_N(t)$ is given by the simple expression

$$S_N(t) \sim At^d \quad [t \ll t_\times] \text{ [regime I]} \tag{3a}$$

where A depends on the lattice. This behaviour should hold so long as the number of accessible sites is much smaller than N or, more precisely, so long as $1/P_{\min}(t) \ll N$, where $P_{\min}$ is the smallest non-zero occupation probability on the lattice at time t. Then $P_{\min}(t) = z^{-t}$, where z is the number of nearest neighbours of a site, so regime I must end at a crossover time $t_\times$ which scales logarithmically with N,

$$t_\times \sim \ln N \tag{3b}$$

Regime I is not present for small N, because it arises from the condition that all the accessible sites must be occupied by many walkers. For large N, the initial growth of the covered territory is very fast, yet the initial growth rate is independent of N (only the duration time $t_\times$ of this regime depends on N).

To discuss times greater than $t_\times$, we calculate $S_N(t)$ from equation (2) using generating function techniques[23-25]. As we are now interested in the long-time behaviour, we use the continuum approximation to evaluate $\Gamma_t(\mathbf{r})$. This analysis leads to a compact scaling expression for $S_N(t)$

$$S_N(t) \sim t^{d/2} f(x) \quad [t \gg t_\times] \tag{4a}$$

Throughout this paper, the tilde ($\sim$) denotes the fact that an equation holds for N and t both large. The scaled variable x is given by

$$x = \begin{cases} N & [d=1] \\ N/\ln t & [d=2] \\ N/\sqrt{t} & [d=3] \end{cases} \tag{4b}$$

and the scaling function $f(x)$ by

$$f(x) = \begin{cases} (\ln x)^{d/2} & t_\times \ll t \ll t_\times' \quad \text{[regime II]} \\ x & t \gg t_\times' \quad \text{[regime III]} \end{cases} \tag{5}$$

Again, these regimes are shown in Fig. 1. Here the second

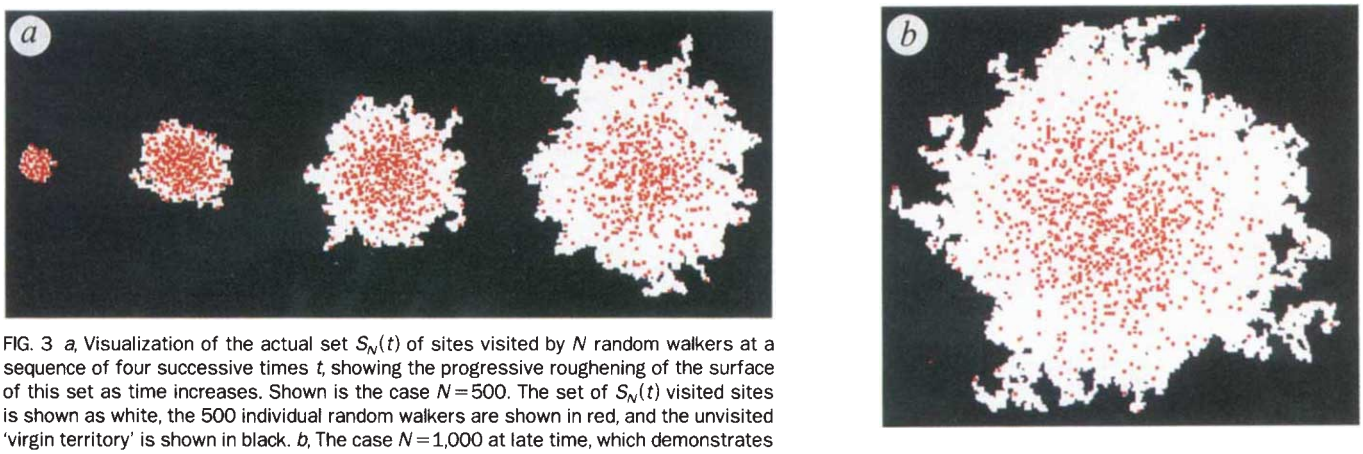

FIG. 3 *a*, Visualization of the actual set $S_N(t)$ of sites visited by N random walkers at a sequence of four successive times t, showing the progressive roughening of the surface of this set as time increases. Shown is the case $N=500$. The set of $S_N(t)$ visited sites is shown as white, the 500 individual random walkers are shown in red, and the unvisited 'virgin territory' is shown in black. *b*, The case $N=1{,}000$ at late time, which demonstrates the part played by only a few individual random walkers in causing the roughening of the interface of the set $S_N(t)$.

crossover time $t'_\times$ is

$$t'_\times \sim \begin{cases} \infty & [d=1] \\ e^N & [d=2] \\ N^2 & [d=3] \end{cases} \qquad (6)$$

The predicted scaling form of equation (4) was tested by extensive calculations using the method of exact enumeration; results are shown in Fig. 2. Note that exact enumerations cannot readily be carried out to times long enough to see regime III because equation (6) implies that $t'_\times$ occurs at fairly large times (especially for $d=2$).

The crossover from regime II to regime III can be understood in the following way. In regime II, the walkers are contained within a d-dimensional sphere of radius $\xi \sim t^{1/2}$ (except for rare fluctuations). Hence $S_N(t)$ must be bounded from above by the volume of this sphere, $V(t) \sim t^{d/2}$. A second upper bound on $S_N(t)$ is $NS_1(t)$, where

$$S_1(t) \sim \begin{cases} t^{1/2} & [d=1] \\ t/\ln t & [d=2] \\ t & [d=3] \end{cases} \qquad (7)$$

is the number of distinct sites visited by one random walker. A crossover in $S_N(t)$ will occur if the system passes from one constraint to the other. For $d=1$, $V(t) < NS_1(t)$ for all t, so no crossover occurs, and regime II holds for arbitrarily large t, confirming the result of equation (6*a*) above. For $d=2$ and 3, we find $V(t) < NS_1(t)$ initially, but for sufficiently large t, $V(t) > NS_1(t)$. Thus $t'_\times$ is obtained from the condition

$$V(t'_\times) \sim NS_1(t'_\times) \qquad (8)$$

For $d=2$, equations (7) and (8) lead to $t'_\times \sim Nt'_\times/\ln t'_\times$, so that $t'_\times \sim e^N$; this confirms the result (6*b*) above. Similarly, for $d=3$, $(t'_\times)^{3/2} \sim Nt'_\times$ implies $t'_\times \sim N^2$, confirming the result (6*c*). Actually, following the same kind of reasoning, we can conclude that the crossover time to the final regime in any dimension higher than 2 will be given by

$$t'_\times \sim N^{2/(d-2)} \qquad [d>2] \qquad (9)$$

This result is a consequence of the fact that $S_1(t) \sim t$ for any dimension larger than 2. One can interpret $t'_\times$ as the time up to which the walkers visit the same places very frequently. For times longer than $t'_\times$, the walkers 'almost' do not see each other, and can be treated independently. Equation (9) shows the effect of the space dimension on $t'_\times$; the higher the dimension, the shorter the times at which walkers become 'independent'.

From Monte Carlo simulations for $d=2$, we find a remarkable transition in the geometry of the set of visited sites. This set initially grows in the shape of a disk with a relatively smooth surface; this occurs at very short times, during regime I. The surface then becomes increasingly rough in regime II (see Fig. 3) as the walkers move further away from one another, until they are so sparse that they can be treated independently; this occurs in regime III. This phenomenon can be linked to $S_N(t)$ by noting that the walkers can find new sites only on the surface of the set of visited sites. Accordingly, the 'growth rate' $\partial S_N(t)/\partial t$ will be proportional to the number of surface sites. For $d=2$ and 3, the number of surface sites increases rapidly as the surface roughens, thus leading to an increase in the growth rate of $S_N(t)$ until it reaches its maximum possible value in regime III. For $d=1$, the surface always consists of two points (the two ends of the set of visited sites), so there is no roughening contribution to the growth rate of $S_N(t)$, which again agrees with the absence of regime III in the one-dimensional case.

The roughening of the surface of the set of visited sites (Fig. 3) can be understood as follows. We denote by $P(r, t)$ the probability that a walker initially at the origin is found at a distance r from the origin at time t. Then the average number of walkers at position r at time t will be given by $NP(r, t)$. In regime I, we have $NP(r, t) > NP_{\min}(t) \gg 1$, so on average all accessible sites are multiply occupied. This set is roughly a sphere of radius t. A different situation occurs in regime II, in which there exists a distance ρ for which $NP(\rho, t) = 1$; for $r > \rho$, the walkers are increasingly sparse. This results in the roughening of the surface of the set of visited sites. Thus regime I is characterized by filling a region of radius $r_1 \sim t$, whereas in regime II there are insufficient walkers to fill more than a region of radius $r_2 \sim \sqrt{t}$. The region between $r_2 \sim \sqrt{t}$ and $r_1 \sim t$ is characterized by walkers who become increasingly isolated from one another with time, leading to an increasingly rough exterior surface. This phenomenon may have been observed by Skellam[13], who plotted contours delineating the advance of the muskrat population, and noted that the contours were initially smooth but later became rough (see Fig. 1 of ref. 13).

Finally, we note that the existence of the different time regimes is a consequence of the initial localization of all N walkers at the origin, which is not an unreasonable assumption in many cases of interest. Suppose, on the other hand, that walkers are initially localized in a box of linear size l. Then we can distinguish three types of behaviour for $S_N(t)$. If $l \ll \xi(t_\times) \sim \sqrt{\ln(N)}$, we expect to observe all three growth regimes of $S_N(t)$. If $\xi(t_\times) \ll l \ll \xi(t'_\times)$, then the system would initially be in regime II, and only the crossover to regime III would occur. If $l \gg \xi(t'_\times)$, then regime III will hold for all times. □

Received 9 October; accepted 5 November 1991.

1. Montroll, E. W. & West, B. J. in *Fluctuation Phenomena* (eds Montroll, E. W. & Lebowitz, J. L.) (North-Holland Personal Library, 1987).
2. Montroll, E. W. & Shlesinger, M. F. in *Nonequilibrium Phenomena II. From Stochastics to Hydrodynamics* (eds Lebowitz, J. L. & Montroll, E. W.) 1-121 (North-Holland, Amsterdam, 1984).

3. Dvoretzky, A. & Erdős, P. in *Proc. 2nd Berkeley Symp.* 33 (University of California, Berkeley, 1951).
4. Vineyard, G. H. *J. math. Phys.* **4,** 1191–1193 (1963).
5. Beeler, R. J. & Delaney, J. A. *Phys. Rev.* A**130,** 962–966 (1963).
6. Beeler, R. J. *Phys. Rev.* A**134,** 1396–1401 (1964).
7. Rosenstock, H. B. *Phys. Rev.* A**187,** 1166–1168 (1969).
8. Montroll, E. W. in *Stochastic Processes in Applied Mathematics* XVI, 193–220 (American Mathematical Society, Providence, 1964).
9. Montroll, E. W. & Weiss, G. H. *J. math. Phys.* **6,** 167–177 (1965).
10. Jain, N. C. & Orey, S. *Israel J. Math.* **6,** 373–380 (1968).
11. Henyey, F. S. & Seshadri, V. *J. chem. Phys.* **76,** 5530–5534 (1982).
12. Torney, D. C. *J. stat. Phys.* **44,** 49–66 (1986).
13. Skellam, J. G. *Biometrika* **38,** 196–218 (1951).
14. Skellam, J. G. *Biometrika* **39,** 346–362 (1952).
15. Pielou, E. C. *An Introduction to Mathematical Ecology* (Wiley-Interscience, New York, 1969).
16. Edelstein-Keshet, L. *Mathematical Models in Biology* (Random House, New York, 1988).
17. Smoluchowski, M. v. *Z. phys. Chem.* **29,** 129 (1917).
18. Rice, S. A. *Diffusion-Controlled Reactions* (Elsevier, Amsterdam, 1985).
19. Haus, J. W. & Kehr, K. W. *Physics Rep.* **150,** 263–416 (1987).
20. Havlin, S. & Ben-Avraham, D. *Adv. Phys.* **36,** 695–798 (1987).
21. Bouchaud, J.-P. & Georges, A. *Physics Rep.* **195,** 127–293 (1990).
22. Bunde, A. & Havlin, S. (eds) *Fractals and Disordered Systems* (Springer, Berlin, 1991).
23. Barber, M. N. & Ninham, B. W. *Random and Restricted Walks* (Gordon & Breach, New York, 1970).
24. Berg, H. C. *Random Walks in Biology* (Princeton University Press, 1983).
25. Weiss, G. H. & Rubin, R. J. *Adv. chem. Phys.* **52,** 363–475 (1983).

ACKNOWLEDGEMENTS. We thank M. Araujo, A. L. Barabasi, G. Huber, J. Lee and P. H. Poole for discussions, and CONACYT, ONR, NSF and the US–Israel Binational Foundation for support.

Crumpled and collapsed conformations in graphite oxide membranes

Xin Wen*, Carl W. Garland*, Terence Hwa†, Mehran Kardar*, Etsuo Kokufuta‡, Yong Li*, Michal Orkisz* & Toyoichi Tanaka*

* Center for Materials Science and Engineering, Massachusetts Institute of Technology, Cambridge, Massachusetts 02139, USA
† Physics Department Harvard University, Cambridge, Massachusetts 02138, USA
‡ Institute of Applied Biochemistry, University of Tsukuba, Tsukuba, Ibaraki 305, Japan

MEMBRANES composed of bilayers of amphiphiles such as phospholipids generally exhibit two-dimensional liquid-like structure within the layers. When the constituent molecules of such a membrane are permanently cross-linked to each other, the membrane becomes less flexible, forming a two-dimensional solid. Solid membranes are expected to exhibit very different behaviour from their liquid counterparts[1–3], including transitions between a two-dimensional flat phase, a crumpled phase of fractal dimension 2.5 and a compact, three-dimensional phase. Experimental evidence for the crumpled phase has, however, been lacking. As this phase was not observed in computer simulations[4–6], it has been suggested that it may always be absent for self-avoiding (and therefore all real) membranes[4–6]. To the contrary, we report here the experimental observation of the crumpled conformation in an aqueous suspension of graphite oxide membranes. Static light scattering measurements indicate the presence of membrane conformations with a fractal dimension of 2.54 ± 0.05. As the intra-membrane affinity is enhanced by changing the composition of the solvent, the membranes collapse to a compact configuration.

A natural state for a solid membrane is a flat configuration. Unlike in a liquid membrane which lacks internal shear elasticity, out-of-plane thermal undulations in a solid membrane are not energetically favoured, because they are accompanied by in-plane strains[2]. When the in-plane elasticity is sufficiently weak or the temperature high enough, it has been argued that a crumpled conformation with random orientations should form because the entropy gain from the increased number of bent and folded configurations more than compensates the internal energy cost[7,8]. Like the coiled polymer, the crumpled membrane is a tenuous fractal[9] with a dimension determined by the competition between the configurational entropy and steric constraints. If the affinity between the molecules is increased, the membrane may collapse completely into a compact configuration[10,11]. Figure 1 provides a schematic representation of these three phases.

In computer simulations[4–6], flat and compact[10,11] conformations have been realized by tuning simple potentials, but the intermediate crumpled phase has not been observed in equilibrium. This has led to the conjecture that a crumpled phase is always absent in self-avoiding membranes[7]. Experimental studies of solid membranes are therefore most desirable. Candidates for solid membranes include sheets of graphite oxide (GO)[12–15] and MoS_2 (ref. 16), the spectrin network extracted from red blood cells (C. Schmitt, personal communication) and polymerized liquid membranes[17]. Previous electron microscope images show that both GO[15] and MoS_2 (ref. 16) form irregular and folded configurations when dried on the microscope stage. Here we study conformations of GO membranes suspended in dilute solution.

GO membranes are synthesized by exfoliating bulk graphite with strong oxidizing agents[12,13,15]; we used potassium permanganate. The product of the oxidation reaction is GO, brownish yellow in colour, which consists of carbon layers bonded by oxygens[14]. Electron microscopy has shown that the GO membranes have a crystalline internal order[15] and can be as thin as one carbon layer[14]. Hydroxyl (OH) groups are bound to the surfaces of the GO membranes[14]. These hydroxyl groups, capable of forming hydrogen bonds with water molecules, are responsible for the compatibility of GO with aqueous solutions.

A light scattering study of the structure of membranes in solution requires some control over their sizes. This was achieved by using polycarbonate filters (Nucleopore). The GO suspension was sequentially passed through filters with 8-μm and 3-μm pore size. The membranes retained on the 3-μm filter were redispersed in a solution, with the original buffer conditions. The final solution contains GO membranes sized between 3 and 8 μm with a concentration of ~0.01 wt%.

In static laser-scattering experiments, conformations of GO membranes are probed through the structure factor, $S(q)$, at a wave vector q, which is directly related to the radius of gyration, R_G, and to the fractal dimension[9], d_f, of the scattering objects. The membrane conformations can be differentiated by their fractal dimensions: for a flat membrane, $d_f = 2$, whereas a compact conformation corresponds to $d_f = 3$. The fractal dimension of the intermediate crumpled phase is estimated to be 2.5, from a Flory argument[3]. For a monodisperse solution[3,18], $S(q) \approx 1 - (qR_G)^2/2$ for $qR_G < 1$, and $S(q) \approx q^{-d_f}$ for $qR_G > 1$. As our solutions are polydisperse, the power law should be checked only at length scales shorter than the size of the smallest GO membranes (3 μm). As our shortest probing length is 0.2 μm (half of the laser wavelength), we have a range of about 1.5 decades in q to determine the scaling exponent d_f for the decay of $S(\mathbf{q})$.

Figure 2 illustrates the structure factors of GO membranes obtained from aqueous solutions at three pH values. The behaviour of $S(q)$ is fairly consistent with a self-similar scaling of density fluctuations at length scales less than the size of membranes. The best fits give a value of $d_f = 2.54 \pm 0.05$, very close to the theoretical estimate[3] of 2.5. The fractal dimension was found to be insensitive to pH and salt concentrations. This is understandable considering the low density of the ionizable groups (one COOH group for every fifty carbons[14]). When 10% acetone is added to the solution, the structure factor, shown in Fig. 3, suggests formation of a compact conformation with a fractal dimension of ~3, and a somewhat smaller radius of gyration. This observation can be explained by the fact that acetone molecules are less polar than water molecules. On addition of acetone, the solvent becomes poorer, and the intra-membrane affinity is enhanced.

Although our observation of a fractal dimension of ~2.5 is consistent with a crumpled phase of membranes, we also consider some other possible explanations. Haphazard crushing of